Research Update: Bismuth-based perovskite-inspired photovoltaic materials

Lana C. Lee, Tahmida N. Huq, Judith L. MacManus-Driscoll, and Robert L. Z. Hoye

Citation: APL Materials **6**, 084502 (2018); doi: 10.1063/1.5029484
View online: https://doi.org/10.1063/1.5029484
View Table of Contents: http://aip.scitation.org/toc/apm/6/8
Published by the American Institute of Physics

APL MATERIALS **6**, 084502 (2018)

Research Update: Bismuth-based perovskite-inspired photovoltaic materials

Lana C. Lee,[1,a] Tahmida N. Huq,[1,a] Judith L. MacManus-Driscoll,[1] and Robert L. Z. Hoye[1,2,b]
[1]*Department of Materials Science and Metallurgy, University of Cambridge, 27 Charles Babbage Rd., Cambridge CB3 0FS, United Kingdom*
[2]*Cavendish Laboratory, University of Cambridge, JJ Thomson Ave., Cambridge CB3 0HE, United Kingdom*

(Received 14 March 2018; accepted 20 April 2018; published online 18 June 2018)

Bismuth-based compounds have recently gained interest as solar absorbers with the potential to have low toxicity, be efficient in devices, and be processable using facile methods. We review recent theoretical and experimental investigations into bismuth-based compounds, which shape our understanding of their photovoltaic potential, with particular focus on their defect-tolerance. We also review the processing methods that have been used to control the structural and optoelectronic properties of single crystals and thin films. Additionally, we discuss the key factors limiting their device performance, as well as the future steps needed to ultimately realize these new materials for commercial applications. https://doi.org/10.1063/1.5029484

I. INTRODUCTION

The effort to find new materials for low-cost thin film solar cells has recently been reinvigorated with the advent of lead-halide perovskites. Photovoltaics based on lead-halide perovskites have exhibited an unprecedented rate of efficiency rise from 3.8% in 2009 to a certified 22.7% in 2017.[1,2] Although the lead-halide perovskites originally investigated (methylammonium lead iodide/bromide) have limited air-stability,[1,3] recently-investigated compositions containing Cs, formamidinium and two-dimensional perovskites have demonstrated over 1000 h device stability.[4,5] However, there is debate over the environmental and commercial impact of the lead content,[6] motivating efforts to find lead-free alternatives.[7]

Many groups searching for lead-free alternatives to lead-halide perovskites have investigated chemical substitution of Pb^{2+} for neighboring elements, such as Sn^{2+}, Ge^{2+}, Sb^{3+}, and Bi^{3+}. These efforts are well-documented in recent reviews, and the compounds are compositionally analogous to lead-halide perovskites, e.g., methylammonium tin iodide, methylammonium germanium iodide, and methylammonium bismuth iodide.[8–11] Another strong emphasis has been on finding compounds with the same crystal structure, resulting in numerous investigations into double perovskites, e.g., $Cs_2AgBiBr_6$, which is also well-documented in recent reviews and articles.[8,12–14] An approach that is contemporary to these is to find compounds that could replicate the tolerance of lead-halide perovskites to intrinsic defects. Computations of methylammonium lead iodide ($CH_3NH_3PbI_3$) have shown that it primarily forms shallow defects, which would lead to low rates of Shockley-Read-Hall recombination.[15] This is thought to be an important factor for lead-halide perovskites to achieve long diffusion lengths enabling high efficiencies, despite their synthesis by defective solution-processing methods.[16] A qualitative model to understand the defect tolerance of lead-halide perovskites is based on their electronic structure. The hybridization of Pb 6*s* and Pb 6*p* orbitals with I 5*p* orbitals leads

[a]L. C. Lee and T. N. Huq contributed equally to this work.
[b]Author to whom correspondence should be addressed: rlzh2@cam.ac.uk

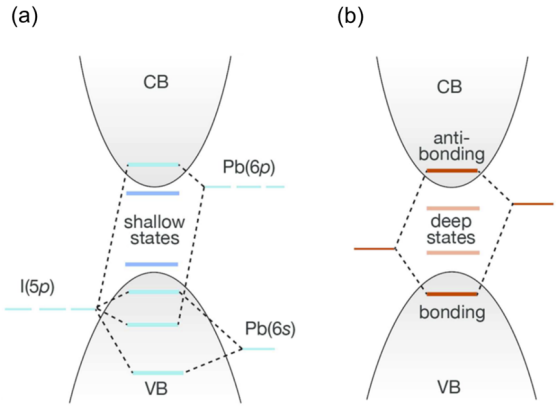

FIG. 1. Illustration of the electronic structure: (a) methylammonium lead iodide, which is defect *tolerant* and (b) a defect *intolerant* compound. CB is the conduction band, and VB is the valence band.[16] Adapted with permission from R. E. Brandt *et al.*, Chem. Mater. **29**, 4667 (2017). Copyright 2017 American Chemical Society.

to the formation of anti-bonding orbitals across the bandgap [Fig. 1(a)]. With this electronic structure, intrinsic defects (e.g., I vacancies) are likely to form close to the band edge or to be resonant within the valence band.[17–19] The energetic distance of defects from the band edge is further reduced by spin-orbit coupling due to the heavy Pb^{2+} cation, which results in greater band-dispersion. This contrasts with the electronic structure of traditional semiconductors, in which the bonding-antibonding orbital pair is formed across the bandgap [Fig. 1(b)]. Dangling bonds from defects in these traditional semiconductors (e.g., GaAs) are then likely to form transition levels close to mid-gap, which lead to high rates of Shockley-Read-Hall recombination.[17,18]

It has been hypothesized that the defect-tolerant perovskite electronic structure could be replicated in materials consisting of a heavy metal cation with a stable pair of valence *s* electrons.[18] Searches through the Materials Genome database for materials with a significant fraction of *s* orbitals in the density of states at the valence band maximum identified bismuth-based compounds as promising.[20] This is because bismuth forms a stable 3+ oxidation state, leading to stable $6s^2$ valence electrons, giving the possibility of replicating the perovskite electronic structure.[18] Bi^{3+} is also a heavy metal cation, and band dispersion due to spin-orbit coupling is expected. In addition, Bi^{3+}, similar to Pb^{2+}, is a large polarizable cation and consequently has a high Born effective charge, leading to high dielectric constants that are important for increased screening of charged defects.[18] Bismuth has the additional important advantage of demonstrating very little evidence of toxicity.[21]

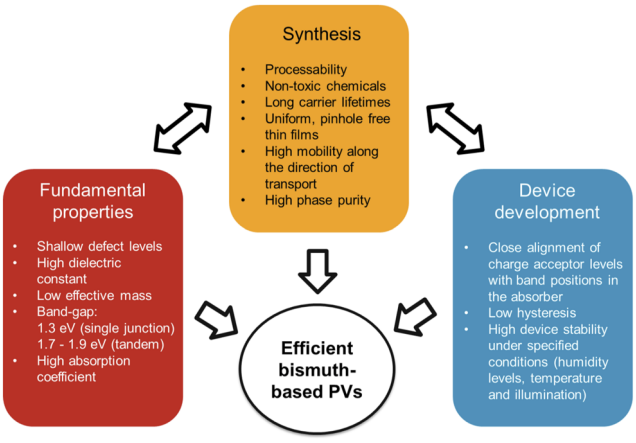

FIG. 2. Summary of the important fundamental materials properties, materials synthesis, and device development considerations for obtaining efficient bismuth-based photovoltaics.

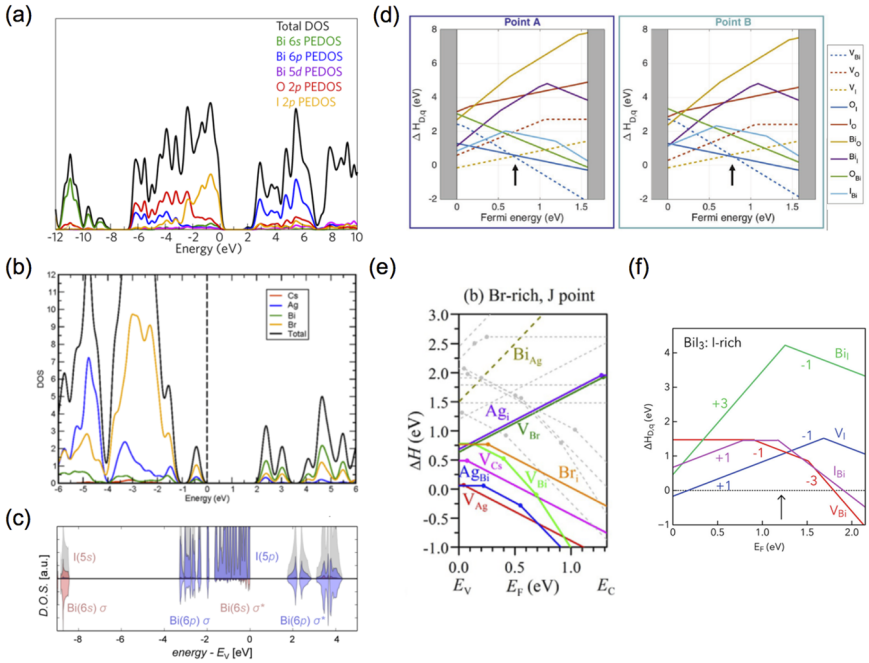

FIG. 3. Computed partial density of states of (a) BiOI,[40] (b) $Cs_2AgBiBr_6$,[41] and (c) BiI_3.[37] Defect calculations of (d) BiOI,[39] (e) $Cs_2AgBiBr_6$,[23] and (f) BiI_3.[16] Reprinted with permission from (a) A. M. Ganose *et al.*, Chem. Mater. **28**, 1980 (2016). Copyright 2016 American Chemical Society; (b) E. T. McClure *et al.*, Chem. Mater. **28**, 1348 (2016). Copyright 2016 American Chemical Society; (c) R. E. Brandt *et al.*, J. Phys. Chem. Lett. **6**, 4297 (2015). Copyright 2015 American Chemical Society; (d) R. L. Z. Hoye *et al.*, Adv. Mater. **29**, 1702176 (2017). Copyright 2017 John Wiley and Sons; (e) Z. Xiao *et al.*, ChemSusChem **9**, 2628 (2016). Copyright 2016 John Wiley and Sons; and (f) R. E. Brandt *et al.*, Chem. Mater. **29**, 4667 (2017). Copyright 2017 American Chemical Society.

In this Research Update, we review recent work exploring bismuth-based compounds for photovoltaics (Fig. 2). We focus not solely on bismuth-based perovskites, but rather on bismuth-based materials that have been identified as promising based on recent defect-tolerance theory. These materials therefore do not necessarily have the perovskite crystallographic structure or a composition similar to lead-halide perovskites but rather are those predicted to replicate the perovskite *electronic* structure (e.g., BiOI and BiSI). We review computations on the electronic structure and defects of these materials to discuss their promise for photovoltaics (Fig. 3). We also evaluate methods to grow these materials and the strategies adopted to improve the morphology, phase-purity, and lifetime. In addition, we review the measured and computed band positions of the materials and early attempts to make solar cells from these new compounds. We conclude with a discussion of the outstanding challenges that need to be addressed as the exploration into bismuth-based photovoltaics matures.

II. THEORETICAL INSIGHTS

Recent in-depth computations of bismuth-based compounds provide important feedback to the selection rules for identifying defect-tolerant absorbers, as well as further insight into the potential of specific materials as solar absorbers. High Born effective charges have been calculated in bismuth-based compounds.[22] The compounds also have high calculated ionic (or static) dielectric constants (Table I). The partial density of states for three such compounds are shown in Fig. 3: BiOI, $Cs_2AgBiBr_6$, and BiI_3. In all three cases, Bi 6*s* states are found in the valence band maximum and they overlap with anion *p* orbitals. Additionally, Bi 6*p* orbitals are found in the conduction band minimum of all three materials, overlapping with the anion orbitals. These electronic structures are consistent with predictions and have also been found in the computed density of states of other bismuth-based

TABLE I. Comparison of the calculated bandgap, effective masses, and ionic dielectric constant with the experimentally measured bandgap of bismuth-based compounds. The highest reported power conversion efficiency and device structure are also included for each material. $CH_3NH_3PbI_3$ is included as a point of reference. Abbreviations used: c-TiO_2 = compact TiO_2, *m*-TiO_2 = mesoporous TiO_2, PTAA = poly[bis(4-phenyl) (2,4,6-trimethylphenyl)amine], spiro-OMeTAD = 2,2′,7,7′-tetrakis(*N*,*N*-di-*p*-methoxyphenyl-amine)9,9′-spirobifluorene, PTB7 = poly({4,8-bis[(2-ethylhexyl)oxy]benzo[1,2-b:4,5-b′]dithiophene-2,6-diyl}{3-fluoro-2-[(2-ethylhexyl)carbonyl]thieno[3,4-b]thiophenediyl}).

Material	Space group	Calculated E_g (eV)	Measured E_g (eV)	m_e/m_0	m_h/m_0	Ionic dielectric constant	Highest PCE (%)	Structure
$CH_3NH_3PbI_3$ (GW-SOC)[a]	*I*4/*mcm* (tetragonal)	1.67[24]	1.55[25]	0.15–0.29[24]	0.18–0.40[24]	20.07[18]	21.2[26]	Glass/FTO/La-$BaSnO_3$/$CH_3NH_3PbI_3$/PTAA/Au[26]
$(CH_3NH_3)_3Bi_2I_9$	$P6_3/mmc$ (hexagonal)[27]	2.0[3,28]	2.9[29]	...	...	...	1.64[30]	FTO/c-TiO_2/m-TiO_2/$(CH_3NH_3)_3Bi_2I_9$/Spiro-OMeTAD/Ag[30]
$(NH_4)_3Bi_2I_9$	$P2_1/c$ (monoclinic)[31]	1.42[31]	2.04[31]	...	...	...	...	...
$K_3Bi_2I_9$	$P2_1/n$ (monoclinic)[22]	2.1[22]	2.1[22]	...	...	...	...	...
$Cs_3Bi_2I_9$	$P6_3/mmc$ (hexagonal)[22]	2.32[22]	1.9[22]	4.63[18]	1.79[18]	9.63[18]	1.09[32]	FTO/c-TiO_2/m-TiO_2/$Cs_3Bi_2I_9$/Spiro-OMeTAD/Ag[32]
$Rb_3Bi_2I_9$	$P2_1/n$ (monoclinic)[22]	2.16[22]	2.1[22]	...	...	[b]	...	...
BiSI	*Pnam* (orthorhombic)[33]	1.78[34]	1.59[35]	0.69–1.78[34]	0.51–0.36[34]	36.8[34]	0.25[36]	FTO/BiSI/NaI and I_2 in acetonitrile/Pt[36]
BiI_3	$R\bar{3}$ (trigonal)[37]	1.93[22]	1.8[22,37]	10.39[18]	1.85[18]	5.70[18]	1.0[38]	FTO/TiO_2/BiI_3/V_2O_5/Au[38]
BiOI	*P*4/*nmm* (tetragonal)[39]	2.0[40]	1.9[39]	0.37[18]	1.9–3.75[40]	37.2–46.32[18,39]	1.8[39]	ITO/NiO_x/BiOI/ZnO/Al[39]
$Cs_2AgBiBr_6$	*Fm* 3*m* (cubic)[41]	2.06[41]	2.19[41]	0.37[41]	0.14[41]	...	2.43[42]	FTO/c-TiO_2/m-TiO_2/$Cs_2AgBiBr_6$/Spiro-OMeTAD/Au[42]
$Cs_2AgBiCl_6$	*Fm* 3*m* (cubic)[41]	2.62[41]	2.77[41]	0.53[41]	0.15[41]	...	...	...
$(CH_3NH_3)_2AgBiBr_6$	$Fm\bar{3}m$ (cubic)[14]	1.3[14]	2.02[14]	0.15–0.86[14]	0.24–1.37[14]	...	...	...
$(CH_3NH_3)_2KBiCl_6$	$R\bar{3}m$[43]	3.02[43]	3.04[43]	...	...	...	...	...
$AgBiS_2$	$P\bar{3}m1$[44] $Fm\bar{3}m$[44]	0.42–1.54[44] 0[44]	0.9[44] ...	0.35[44] ...	0.72[44] ...	17.3–19.3[44] ...	6.3[45]	ITO/ZnO/$AgBiS_s$/PTB7/MoO_3/Ag[45]

[a]SOC is spin orbit coupling.

[b]We note that the *electronic* dielectric constant of $Rb_3Bi_2I_9$ has been computed ranging from 19.3 to 65.5.[22]

compounds, such as BiSI[18] and $(CH_3NH_3)_3Bi_2I_9$.[3] However, the contribution of the Bi 6*s* orbitals to the valence band maximum in these materials is smaller than Pb 6*s* orbitals in $CH_3NH_3PbI_3$,[18] resulting in less cation-anion orbital interaction. Since the dispersion of the valence band maximum depends on orbital interactions, the effective mass for holes is higher than in $CH_3NH_3PbI_3$, as shown in Table I, indicating that the mobility of holes is lower in bismuth-based compounds.[16] This effect is particularly pronounced in $Cs_2AgBiBr_6$ double perovskite, in which the contribution of Ag 4*d* orbitals exceeds that of the Bi 6*s* orbitals (Fig. 3). The directionality of the Ag 4*d* orbitals results in the Ag 4*d* and Bi 6*s* states having high charge density at different *k*-points in the conduction band minimum, giving a flatter conduction band and wider bandgap than $CsPbBr_3$.[12] This results in higher effective masses.[12,23] The mixing of Br *p* orbitals with Ag d_z^2 orbitals at the X point in reciprocal space results in the valence band maximum occurring at the X point rather than at the L point (where the conduction band minimum is), giving an indirect bandgap. Calculations have shown that the lower absorption coefficients resulting from the indirect bandgap limit the maximum achievable efficiencies.[12]

Defect calculations have also shown that not all bismuth-based compounds with *s* orbitals at the valence band maximum form shallow defects. Transition levels are Fermi energies at which there is a change in the charge of a defect and are energies within the bandgap at which a defect is expected to be able to trap electrons or holes. The concentration of a defect decreases with the exponent of formation energy and has an Arrhenius relationship with temperature. A formation energy above 1-1.5 eV can be considered high enough for the concentration of a defect to be neglected if the material is grown at temperatures of up to 600 K.[16] In the case of BiOI, the formation energies of all transition levels computed were >1.5 eV [Fig. 3(d)].[39] This indicates that BiOI is tolerant to all anti-site and vacancy defects investigated since deep transition levels are not expected to be present. However, for $Cs_2AgBiBr_6$, low formation-energy transition levels have been found [Fig. 3(e)].[23] Although some of these defects are shallow (e.g., silver vacancies), other defects have transition levels close to mid-gap that would be expected to give high rates of Shockley-Read-Hall recombination. For example, the Ag_{Bi} anti-site defect has a deep −1/−2 charge transition level located 0.55 eV from the valence band maximum.[23] In part, these deeper traps are due to the reduced and more localized orbital overlap in the valence band maximum, which results in a wider bandgap.[12] Deep traps have also been found in BiI_3, such as the −1/−3 transition level, located >0.5 eV from the conduction band minimum, with a formation energy of <1 eV [Fig. 3(f)].[16]

The crystal structure also strongly influences the electronic structure, in particular the effective mass. Figure 4 compares three bismuth-based compounds with different dimensionalities. $(CH_3NH_3)_3Bi_2I_9$ has a crystallographic dimensionality of 0.5D because the $[BiI_6]^{3-}$ octahedra occur as face-sharing pairs that form isolated $Bi_2I_9^{3-}$ groups, which alternate with $CH_3NH_3^+$ cations [Fig. 4(a)].[3,27] By contrast, a 0D material would have completely isolated octahedra, whereas a 1D material would have isolated ribbons of bismuth halide. The low dimensionality of $(CH_3NH_3)_3Bi_2I_9$ limits charge transport because electrons and holes tend to be localized in the isolated $Bi_2I_9^{3-}$ groups, resulting in flat bands in the valence band maximum and low dispersion in the conduction band minimum [Fig. 4(b)].[28] Higher dispersion and lower effective masses occur in BiOI, which has a two-dimensional Matlockite structure [Fig. 4(c); Table I].[18,40] $Cs_2AgBiBr_6$, which has 3D crystallographic symmetry, has higher dispersion still, with the lowest effective masses of 0.14 for holes along the X-Γ direction or 0.37 along the R-X direction, and 0.37 for electrons along the L-W direction in reciprocal space.[41] However, these effective masses are not as low as found in $CH_3NH_3PbI_3$, in part due to reduced orbital overlap. Recently, Yan *et al.* introduced the concept of electronic dimensionality to describe the connectivity of the orbitals in the upper valence band and lower conduction band. This accounts for the reduced orbital overlap in $Cs_2AgBiBr_6$, which gives an electronic dimensionality that is of lower order than the crystallographic dimensionality.[29] To illustrate this point, Yan *et al.* made computations for the more extreme case of Cs_2SrPbI_6, which has 3D crystallographic dimensionality but an electronic dimensionality of 0D because the $[SrI_6]^{3-}$ octahedra do not contribute to the density of states at the band edge. This results in the Pb 6*s* and I 5*p* orbitals from the $[PbI_6]^{3-}$ octahedra being isolated, giving flatter bands and a wider bandgap.[29]

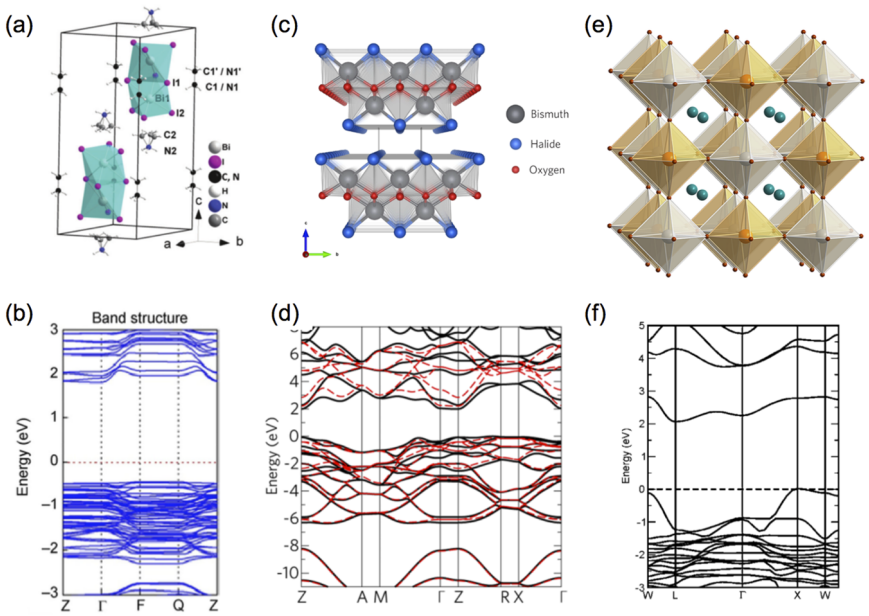

FIG. 4. Experimental crystal structure and calculated band structure of (a) and (b) $(CH_3NH_3)_3Bi_2I_9$,[27,28] (c) and (d) BiOI,[40] and (e) and (f) $Cs_2AgBiBr_6$.[13,41] Reprinted with permission from (a) K. Eckhardt *et al.*, Chem. Commun. **52**, 3058 (2016). Published by the Royal Society of Chemistry; (b) M. Lyu *et al.* Nano Res. **9**, 692 (2016). Copyright 2016 Springer Nature; [(c) and (d)] A. M. Ganose *et al.*, Chem. Mater. **28**, 1980 (2016). Copyright 2016 American Chemical Society; (e) A. H. Slavney *et al.*, J. Am. Chem. Soc. **138**, 2138 (2016). Copyright 2016 American Chemical Society; and (f) E. T. McClure *et al.*, Chem. Mater. **28**, 1348 (2016). Copyright 2016 American Chemical Society.

III. GROWTH OF BISMUTH-BASED MATERIALS FOR PHOTOVOLTAICS

Although photovoltaic devices ultimately require the bismuth-based compounds to be synthesized as pinhole-free thin films, new materials are often initially investigated as single crystals. Single crystal diffraction allows the precise determination of the crystal structure and atomic position. Single crystals can in some cases also achieve lower trap densities, at the very least due to the absence of grain boundaries, allowing the mobility and lifetime limits to be investigated. These findings help to determine whether the material possesses suitable properties for photovoltaics before more research-intensive development of devices is undertaken. Two common methods for single-crystal synthesis are the vertical Bridgman method and the solvothermal method [Figs. 5, 6(a), and 6(b)]. In the former, a material is heated above its melting point and cooled slowly from one end of the container to aid slow recrystallization. A seed crystal can be used, the crystallographic orientation of which will determine the orientation of the resultant single crystal. For the solvothermal method, a solution of precursors is heated in a sealed autoclave. A temperature gradient across the chamber aids the crystallization of the product from solution as single crystals, due to the difference in solubility of the product in solution at different temperatures. Single crystal bismuth compounds have previously been grown using this method for application in scintillators, X-ray detectors, and as ferroelectric materials.[46–51] Here, we review the techniques that have been used to grow and characterize single crystals of a selection of bismuth-based compounds, before discussing thin film synthesis. The learnings from these materials can be applied to new bismuth-based compounds that researchers may wish to fabricate.

A. Single crystals

Single crystal diffraction methods have been used to identify the structure of methylammonium bismuth iodide, $(CH_3NH_3)_3Bi_2I_9$, single crystals. In early work by Jakubas *et al.*, $(CH_3NH_3)_3Bi_2I_9$ single crystals were assigned to the space group $P6_3/mmc$ using Weissenberg photographs.[52] Eckhardt *et al.* recently confirmed this structure through single crystal diffraction.[27] Both groups deduced that $(CH_3NH_3)_3Bi_2I_9$ consists of isolated $Bi_2I_9^{3-}$ clusters as opposed to the corner sharing metal-halide octahedra that are found in $CH_3NH_3PbI_3$. In temperature-dependent optical studies of

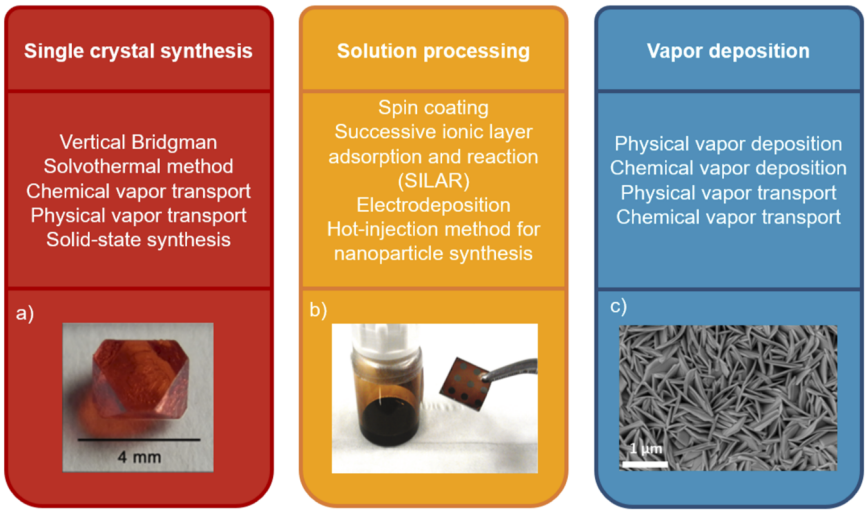

FIG. 5. Summary of growth techniques used for single crystals and thin films of bismuth-based compounds and images of (a) $Cs_2AgBiBr_6$ single crystal from concentrated HBr by solvothermal growth,[13] (b) thin film of $AgBiS_2$ nanocrystals alongside the nanocrystal precursor solution,[45] and (c) a scanning electron microscopy (SEM) image of a BiOI thin film grown by chemical vapor transport.[39] Images reproduced with permission from (a) A. H. Slavney *et al.* J. Am. Chem. Soc. **138**, 2138 (2016). Copyright 2016 American Chemical Society; (b) M. Bernechea *et al.*, Nat. Photonics **10**, 521 (2016). Copyright 2016 Springer Nature; and (c) R. L. Z. Hoye *et al.*, Adv. Mater. **29**, 1702176 (2017). Copyright 2017 John Wiley and Sons.

$(CH_3NH_3)_3Bi_2I_9$,[53] Kawai *et al.* observed an excitonic peak centered at 2.51 eV, which they attributed to localized electronic states on the $Bi_2I_9^{3-}$ clusters. They calculated an exciton binding energy of 300 meV, which is much larger than the exciton binding energy of 5 meV reported for $CH_3NH_3PbI_3$.[54] Abulikemu *et al.*[55] reported the synthesis of $(CH_3NH_3)_3Bi_2I_9$ single crystals from reaction precursors in concentrated HI, with recrystallization from an anti-solvent. An indirect bandgap of 1.96 eV was determined, although the excitonic nature of the material was not considered in the bandgap measurement. From space charge limited current measurements, a trap state density of 3.3×10^{11} cm^{-3} was measured, an order of magnitude higher than for $CH_3NH_3PbI_3$ single crystals, but it is not known whether these traps are deep or shallow.[56] The high trap density, wide bandgap,

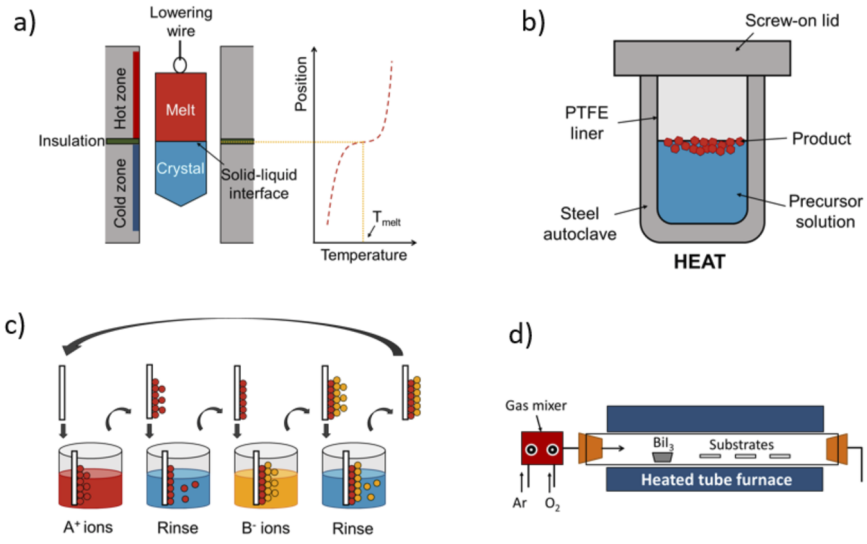

FIG. 6. Diagrams detailing the growth method for the (a) vertical Bridgman method, (b) solvo-/hydro-thermal method, (c) successive ionic layer adsorption and reaction (SILAR), and (d) chemical vapor transport.

and high exciton binding energy limiting free-carrier generation altogether may limit the application of $(CH_3NH_3)_3Bi_2I_9$ as a solar absorber.

Single crystals of bismuth sulphoiodide (BiSI), a chalcohalide with 1D crystallographic dimensionality,[34] have been fabricated by hydrothermal, solvothermal, Bridgman-Stockbarger, and vapor growth methods.[51,57–60] Indirect bandgaps of 1.55–1.61 eV have been reported for the rod-like crystals which are more suitable for single-junction solar cells than the wider bandgap $(CH_3NH_3)_3Bi_2I_9$.[57] BiSI has been assigned to the *Pnam* space group through X-ray diffraction studies, with the structure consisting of covalently bonded $([BiSI]_\infty)_2$ ribbons held together by *van der Waals* interactions between the ribbons.[33,34] Density functional theory (DFT) calculations predict anisotropic conductivity, with higher mobility along the ribbons (covalent bonds) than between them (weaker *van der Waals* interactions), suggesting controlled vertical growth of BiSI is key for good charge transport in devices.[34] However, there are limited experimental studies on the transport properties of single crystals, which would be useful to determine the defect tolerance of the material (as well as mobility and lifetime limits).

For materials with 2D crystallographic dimensionality, BiI_3 single crystals have been grown by several methods including the (modified) vertical Bridgman method and physical vapor transport.[37,61,62] Due to the indirect nature of the bandgap resulting in a low absorption coefficient near the band edge (10^2 cm^{-1}), measurements by ellipsometry have resulted in an overestimation of the bandgap where the direct transition was probed (~1.9 eV).[61] Through optical absorption measurements, an indirect bandgap at 1.67–1.73 eV has been observed.[61] Measuring single crystals grown by an electrochemical gradient vertical Bridgman method, Brandt *et al.* reported a photoluminescence emission centred at 1.85 eV.[37] From time-resolved photoluminescence measurements, they estimated a minority carrier lifetime of 1.3–1.5 ns. This is above the 1 ns lifetime threshold for absorbers worth further investigation as thin films and devices.[16,63] Previously, Dmitriyev *et al.* reported an electron mobility-lifetime ($\mu_e\tau_e$) product of 9.5×10^{-6} cm V^{-1} for BiI_3 single crystals grown by the Bridgman method, equating to a diffusion length of 4.9 μm which is on a comparable length to $CH_3NH_3PbI_3$ perovskite single crystals.[56,64] This value was larger than the $\mu_e\tau_e$ product recorded for single crystals grown by physical vapor transport, for which Saito *et al.* measured values of 3.4–8.5 $\times 10^{-6}$ cm V^{-1}.[62] Han *et al.* reported a route to improve the electron mobility of BiI_3 from 600 cm^2 V^{-1} s^{-1} to 1000 cm^2 V^{-1} s^{-1} via Sb-doping (determined from time-of-flight measurements).[65] They identified I-vacancies as the major defect in BiI_3 and using DFT calculations proposed that Sb-doping increases the formation energy of iodine vacancies, thus reducing iodine migration through BiI_3. However, BiI_3 has a large hole effective-mass of 10.39 (Table I), whilst also being known to suffer from severe hole trapping, thus its application in devices may be limited by poor hole transport.[18,65]

BiOI is another 2D material that has generated interest as a solar absorber based on its promising activity as a photocatalyst.[66] BiOI single crystals have been grown by chemical vapor transport, where their application as a substrate in superconductor devices was studied.[67] Electrical measurements showed that BiOI increased in conductivity by 1.65×10^{-7} S at 275 K when excited by a laser with a wavelength of 640 nm excitation, demonstrating potential as a photoactive material.[68]

The most common 3D bismuth-based compounds investigated are double perovskites. Volonakis *et al.* synthesized $Cs_2BiAgCl_6$ single crystals by solid-state synthesis in a heated ampoule.[69] A time constant of 100 ns was fitted to the tail of the photoluminescence decay measurements; however the material possessed an indirect bandgap of 2.3-2.5 eV, which is too large to achieve reasonable conversion efficiencies in a single-junction solar cell. Slavney *et al.* were able to reduce the bandgap through synthesis of the brominated analog, $Cs_2BiAgBr_6$, by heating the precursors in concentrated HBr.[13] The material demonstrated weak photoluminescence emission, but the time resolved photoluminescence measurements exhibited a long tail, which was attributed to the fundamental lifetime of the material. Fitting the photoluminescence decay, the time constant of this tail was found to be 667 ns, which is comparable to the lifetimes of lead-halide perovskites, but we note that the intensity decreased by 1-2 orders of magnitude before reaching the tail in the decay. A recent investigation by Hoye *et al.* found that the photoluminescence in $Cs_2AgBiBr_6$ was weak (0.01% photoluminescence quantum efficiency) and red-shifted to the optical bandgap. Optical, transient absorption and photoemission spectroscopy measurements strongly suggested that the photoluminescence decay related to recombination to defect states in the band-gap, rather than across the indirect bandgap.[111] While no standard

protocol for stability measurements of single crystals exists, thermogravimetric analysis (TGA) measurements showed that the material was stable at temperatures up to 430 °C, while differential thermal analysis showed no phase transitions in this temperature range. Both factors are important as the operating temperature of solar panels can reach >60 °C. McClure *et al.*[41] measured an indirect bandgap of 2.19 eV for $Cs_2BiAgBr_6$ by diffuse-reflectivity measurements and observed improved phase purity for single crystals synthesized from acid as opposed to solid-state synthesis. The bandgap of $Cs_2AgBiBr_6$ was further reduced to 1.4 eV (indirect) and 1.6 eV (direct) by alloying with Tl, with the composition $Cs_2(Ag_{1-a}Bi_{1-b})Tl_xBr_6$ ($x = a + b$).[13] A Tl content of $x = 0.074$ gave the minimum bandgap. However, Tl is more toxic than Pb. Du *et al.*[70] also demonstrated bandgap tuning of the double perovskites by alloying $Cs_2BiAgBr_6$ with In^{III} and Sb^{III}. Sb^{III} substitution resulted in an indirect bandgap reduction from 2.12 eV to 1.85 eV at 37.5% Sb^{III}. However, sub-bandgap peaks dominated the photoluminescence spectrum due to deep defect states introduced by the dopant. In^{III} doping resulted in a stronger photoluminescence signal than the un-doped material; however, the bandgap increased from 2.12 eV for pure $Cs_2BiAgBr_6$ to 2.27 eV for 75% In^{III} substitution. Calculations have shown that another method for reducing the bandgap of $Cs_2AgBiBr_6$ is through disorder between Ag^+ and Bi^{3+} cations, which have similar ionic radii, although there is a reduction in band dispersion, and disordering may lead to reduced mobilities.[71]

B. Thin films

The properties of thin films vary over a wide range, depending on their processing. In the exploration of bismuth-based compounds, much of the effort has focused on eliminating pinholes (which can act as shunt pathways) and controlling the structural properties (e.g., preferred orientation and achieving large grains), which influence the optoelectronic properties (e.g., mobility and lifetime). The fundamental principles of thin film growth are well-documented by Thompson and other authors,[72–75] and common solution-based and vapor-based growth methods are listed in Fig. 5.

For $(CH_3NH_3)_3Bi_2I_9$, Park *et al.* reported synthesis via a one-step spin casting method.[32] Films demonstrated weak photoluminescence emission and had poor morphology, consisting of interlinked, overlapping grains. Substitution of $CH_3NH_3^+$ with Cs^+ resulted in an increase in the photoluminescence quantum yield; however, this caused the bandgap to increase. Öz *et al.* also found that $(CH_3NH_3)_3Bi_2I_9$ films processed by a one-step spin casting method had poor morphology.[76] Difficulty in achieving compact $(CH_3NH_3)_3Bi_2I_9$ films has been attributed to the fast crystallization and the poor solubility of BiI_3 in common organic solvents.[77] Hoye *et al.* proposed two-step fabrication processes to improve the quality of the films.[3] BiI_3 was first spin-cast and annealed, followed by the diffusion of methylammonium iodide through either spin-casting on top or through exposure to methylammonium iodide vapor inside a vacuum oven. The films processed through vapor-assisted conversion demonstrated longer lifetimes. A further increase in lifetime to a value of 8.1 ns was achieved by exposing the thin films to pyridine.[3,16] The longer lifetimes may have been due to the passivation of surface states (reduced surface recombination) and possibly reduced structural defects in the bulk of the film when processed at higher temperatures through vapor reaction. Two-step growth of compact $(CH_3NH_3)_3Bi_2I_9$ thin films using evaporation steps has also been demonstrated.[30,78] However, photoluminescence lifetimes were limited at 2.84 ns. Additionally, the vacuum processing routes are limited by long processing times. Shin *et al.* recently presented a solution-processing route to compact phase-pure $(CH_3NH_3)_3Bi_2I_9$ films using a solvent engineering approach with antisolvent dripping to further aid recrystallization during the spin-casting process.[77] Infra-red measurements showed that adding dimethyl sulfoxide (DMSO) or 4-*tert*-butyl pyridine (tBP) as additives to solutions of BiI_3 and methylammonium iodide resulted in the formation of additive-BiI_3 Lewis adducts, which improved the solubility of BiI_3 and slowed down the crystallization process. $(CH_3NH_3)_3Bi_2I_9$ films had a similar grain size to those produced by a two-step process with a vacuum step by Ran *et al.*;[78] however, by comparing SEM images, the films produced by the solvent-engineering approach appear more compact and continuous, contributing toward higher device power conversion efficiencies (0.71% *vs.* 0.39%). Despite these efforts to achieve compact thin films, the short-circuit current densities have been below 2.95 mA cm^{-2}.[30] While this is partly due to the wide bandgap of 2.9 eV in $(CH_3NH_3)_3Bi_2I_9$,[29] the high effective masses (Table I) and high exciton binding energy could also limit the mobility and diffusion length of carriers (Sec. II).

Tuning the bandgap of the bismuth chalcohalides is possible by substituting the chalcogenide or halide species.[34] Kunioku *et al.*[35] reported the synthesis of BiSI thin films, with rod like grains 200–500 nm in size, by treating BiOI with H_2S at ambient pressure and 150 °C. The bandgap reduced from 1.96 eV to 1.59 eV, making it more suitable for a single-junction solar cell. However, careful control is needed when using H_2S due to its toxicity (exposure limit of 5 ppm). Additionally, the rods were randomly aligned. According to band structure calculations, vertically oriented crystals between charge transport layers should be optimal for charge transport due to the smaller electron and hole effective masses along this pathway.[34] Controlling the growth direction of BiSI will be important to achieve high device performance. Kunioku *et al.* also reported that the bandgap of BiOI can be further reduced to <1.37 eV by treatment with H_2Se gas to form BiSeI. However, H_2Se is more toxic than H_2S with an exposure limit of 0.05 ppm, which could restrict commercialization. It should be noted that the substitution of iodine with lighter halide species causes widening of the bandgap; therefore, BiOX where X = F, Cl, or Br are likely to be unsuitable for photovoltaic absorbers.[40]

Brandt *et al.* reported the growth of compact BiI_3 thin films by physical vapor transport and solution-processing.[37] Physical vapor transport-grown films had large grains perpendicularly oriented to the substrate while solution processing produced smaller grains. Photoluminescence lifetimes of 180–230 and 190–240 ps were fit for physical vapor transport and spin-cast films, respectively, an order of magnitude shorter than the single crystal lifetimes. By growing films by physical vapor transport at higher temperatures (250 °C *vs.* 160 °C, with the homologous temperature increasing from $0.63T_m$–$0.77T_m$, the same group measured an improvement in the effective lifetime to 7.3 ns.[16] These efforts indicate that BiI_3 is not defect-tolerant, since a high-quality material needs to be synthesized in order to achieve lifetimes >1 ns, and this agrees with the defect calculations (Sec. II). It has also been challenging to achieve compact, pinhole-free thin films of BiI_3.[37] Two contemporary investigations of BiI_3 devices based on solution-processed thin films reported open-circuit voltages >1.3 V below the bandgap with low shunt resistances, and pinholes in the thin films may contribute to this shunting.[38,79]

As well as single crystals, thin films of BiOI, with an indirect bandgap ~1.9 eV,[35,39] have been synthesized for photovoltaic and photocatalytic applications by methods such as successive ionic layer adsorption and reaction [SILAR, Fig. 6(b)][80] and the solvothermal method.[81] Films fabricated by SILAR were non-compact, with crossed grains, which exposed leakage pathways, whilst those produced by the solvothermal method consisted of microspheres containing small BiOI particles. In both cases, poor photo-currents and voltages were reported in solar cells. We recently reported the growth of BiOI by chemical vapor transport [Fig. 6(d)].[39] Films were more compact than those fabricated by SILAR, and a photoluminescence lifetime of 2.7 ns was measured. These BiOI thin films were also shown to be stable in air for the duration of the 197-day experiment, when the relative humidity varied from 45% to 67%.[39]

There are few reports of double perovskite thin films, owing to difficulties in dissolving the precursors in a common organic solvent. The first report is from Greul *et al.*,[42] who fabricated $Cs_2BiAgBr_6$ by a one-step spin casting method. A photoluminescence decay which had a tail with a time constant of 220 ns was measured, which, whilst shorter than that measured for single crystal $Cs_2BiAgBr_6$, is up to two orders of magnitude longer than the lifetimes reported for most thin film bismuth-based compounds. But again we note that a recent investigation has found that the photoluminescence in $Cs_2AgBiBr_6$ originates from defect emission rather than across the band-gap. Hoye *et al.* directly tracked the decay of all photo-carriers in their $Cs_2AgBiBr_6$ thin films by transient absorption spectroscopy and found the lifetime of carriers recombining across the indirect band-gap to be 1.4 μs. This was two orders of magnitude slower than the photoluminescence decay.[111] Whilst the bandgap is too large for single-junction solar cells, it is suitable for a top-cell in 4-terminal tandem devices on silicon, but the low absorption coefficient may limit the achievable efficiencies.[82]

$AgBiS_2$ thin films have also been investigated for photovoltaic applications. Although the lowest-energy room-temperature polymorph of $AgBiS_2$ is the hexagonal matildite structure, nanocrystals of $AgBiS_2$ have been reported to form a rock-salt structure.[45] $AgBiS_2$ has been employed in semiconductor-sensitized solar cells as a replacement for PbS. Thin films of $AgBiS_2$ have been fabricated by SILAR,[83] electrochemical atomic layer deposition,[84] and from solution processing of nanocrystals synthesized by the hot injection method.[85] For the former two, the devices had

low open-circuit voltages and fill factors due to incomplete coverage of the electron transport layer exposing recombination pathways, while the latter used insulating ligands to cap $AgBiS_2$ nanocrystals.[45] Recently, Bernechea *et al.*[45] showed that through tetramethylammonium iodide treatment of nanocrystal thin films, the average device efficiency improved threefold from 1.5% to 4.8% (with a champion certified device efficiency of 6.3%, Table I), the highest recorded efficiency for any of the bismuth compounds discussed. This work highlights the importance of exploring strategies to passivate defects when investigating new bismuth-based compounds.

IV. CONTACTS AND DEVICE PERFORMANCE FOR BISMUTH-BASED PHOTOVOLTAICS

The architectures investigated for bismuth-based photovoltaics are often borrowed from lead-halide perovskite devices. These device structures are summarized in recent reviews,[10,11] and typically comprise of *n-i-p* and *p-i-n* planar stacks [Figs. 7(a) and 7(b)].[86] The *n*-type electron-transport layer (ETL) and *p*-type hole transport layer (HTL) typically have wider bandgaps than the intrinsic absorber (*i* layer) to avoid parasitic absorption. The advantage of these architectures is that the internal electric field occurs over the entire absorber layer [Fig. 7(c)]. This aids charge separation and extraction through drift, which is particularly important for absorbers with short diffusion lengths. By comparison, in heterojunction devices, drift occurs in the depletion region and diffusion in the quasi-neutral region.[87] The highest reported device efficiencies of a selection of bismuth-based photovoltaics and their device structures are given in Table I. Some of the reviews detailing device optimization efforts are given in Refs. 8, 10, and 11 but it is clear that in most cases the efficiencies are not close to reaching or exceeding 10%. While some of the reasons for the limited photovoltaic performance are intrinsic to the materials (discussed in Secs. II and III), other reasons are the sub-optimal band-alignment between the bismuth-based absorbers and charge extraction layers.

Efficient device operation requires that the hole and electron transport layer charge extraction levels are energetically matched with the valence and conduction bands of the absorber, respectively. The conduction (valence) band of the hole transport layer (electron transport layer) must also block electrons (holes). In bismuth-based compounds, this is challenging owing to their deep valence band maxima. The ionization potentials in bismuth-based compounds tend to be higher than in $CH_3NH_3PbI_3$ because the higher atomic number of Bi^{3+} attracts the 6*s* orbital to deeper energies than occurs with Pb^{2+}. The computed band positions of some bismuth-based compounds are shown in Fig. 8, with experimentally measured positions in Fig. 9. For bismuth-based materials, the valence band maximum ranges from −5.2 eV to −7.03 eV relative to a vacuum. By comparison, $CH_3NH_3PbI_3$ has a valence band maximum at −5.43 eV.[88] $(CH_3NH_3)_3Bi_2I_9$, with a valence band maximum at −5.9 eV, is one of the most commonly investigated bismuth-based compounds.[3] Shin *et al.*[77] recently demonstrated that the efficiency of $(CH_3NH_3)_3Bi_2I_9$ solar cells could be improved by

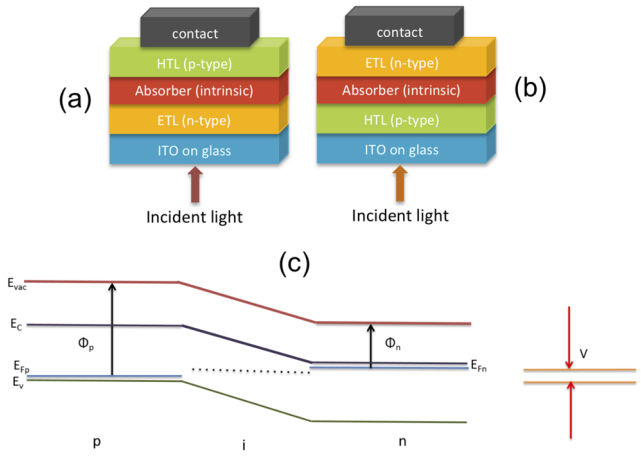

FIG. 7. Illustration of (a) *n-i-p* and (b) *p-i-n* device stacks. (c) Band alignment of an ideal *p-i-n* device stack under short circuit conditions.

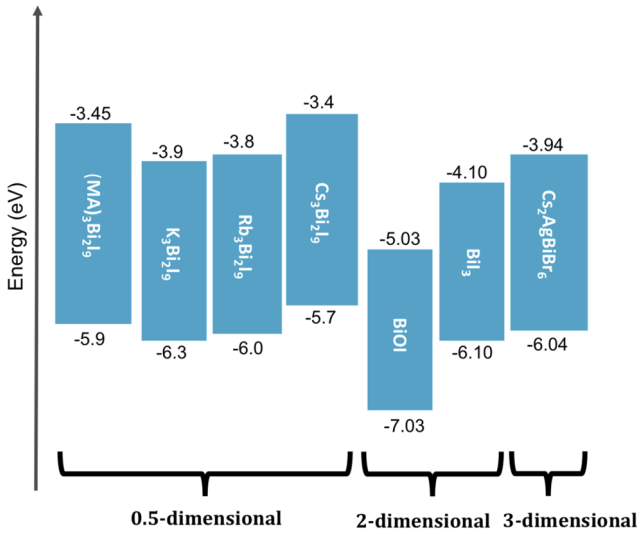

FIG. 8. Computed band positions of bismuth-based absorbers relative to the vacuum level.

replacing spiro-OMeTAD (2,2′,7,7′-tetrakis(N,N-di-*p*-methoxyphenyl-amine)9,9′-spirobifluorene), an organic hole transport layer commonly used in lead-halide perovskite devices, with PIF8 TAA (poly-indenofluoren-8-triarylamine), which has a deeper highest occupied molecular orbital (HOMO) level which is more closely aligned with the valence band maximum of $(CH_3NH_3)_3Bi_2I_9$. BiOI is another example where the device performance has been shown to be limited due to sub-optimal band alignment, in which downward band bending of BiOI occurs at the interface with the NiO_x hole transport layer.[39] In a study by Greul *et al.*[42] on $Cs_2AgBiBr_6$ double perovskite devices, the large band offset between the spiro-OMeTAD (−5.13 eV) and $Cs_2AgBiBr_6$ (−6.04 eV) has been highlighted as one of the main barriers for limited V_{OC} and inefficient charge extraction. It is therefore important to find new hole transport materials for bismuth-based compounds. However, commonly used organic hole transport layers have non-ideal HOMO levels (−5.2 to −5.3 eV).[76] Furthermore, common additives, such as 4-*tert*-butylpyridine, can dissolve the absorber.[89] Organic materials are also prone to degradation (potentially limiting device lifetime), are expensive,[90,91] and have been found to be the source of failure in fracture toughness testing.[92] Possible inorganic alternatives include *p*-type NiO_x doped with Li or Cu.[93,94] MoO_3, an *n*-type compound with a conduction band maximum at −6.4 eV can also be used for hole extraction,[95] although MoO_3 has been reported to degrade $CH_3NH_3PbI_3$.[96] Another class of potential hole transport layers are two-dimensional metal chalcogenides, such as MoS_2 and WS_2. These have the advantage of high carrier mobilities (approx. 200 $cm^2\ V^{-1}\ s^{-1}$ and 50 $cm^2\ V^{-1}\ s^{-1}$ for MoS_2 and WS_2, respectively)[97,98] and tuneable work functions.[99–101]

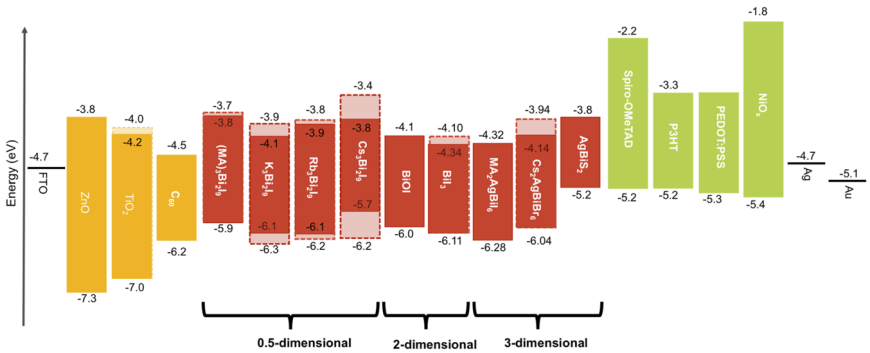

FIG. 9. Measured band positions of electron transport layers (yellow), bismuth-based absorbers (red), and hole transport layers (green). We categorized the bismuth-based absorbers by crystallographic dimensionality. As explained in Sec. II, this can influence charge transport. Note that MA = $CH_3NH_3^+$.

For electron transport layers, bismuth-based photovoltaics commonly use *n*-type oxides, such as TiO_2, SnO_2, and ZnO, which have given the most efficient lead-halide perovskite devices.[102] The conduction band minima of these *n*-type oxides (between −3.4 eV and −4.5 eV) are well aligned with the conduction band minima of the bismuth-based absorbers. Additionally, the oxide electron transport layers can be constructed into mesoporous scaffolds. Meso-superstructured devices, particularly those using mesoporous TiO_2, have enabled record efficiencies in lead-halide perovskites.[103] The advantage of mesoporous scaffolds is that the transport length required for photogenerated electrons from the absorber to reach the electron transport layer is reduced since the nanocrystalline oxide penetrates into the bulk of the absorber layer.[104] This advantage is clearly exhibited in the investigation by Zhang *et al.* where planar TiO_2 with $(CH_3NH_3)_3Bi_2I_9$ yielded a device efficiency of 0.14%, whereas mesoporous TiO_2 on top of a compact layer exhibited an efficiency of 0.42%.[104] In light of this, mesoporous TiO_2 continues to be the most widely used electron transport layer, and the efficiency of $(CH_3NH_3)_3Bi_2I_9$ devices has reached 1.6% utilising this workhorse electron transport material.[30] Amongst other oxides, planar ZnO has been exploited in devices based on BiOI[39] and $AgBiS_2$.[45] ZnO has a conduction band minimum located at −3.8 eV, but it is yet to be fully explored with new classes of bismuth-based absorbers.

V. OUTLOOK

An important limitation of bismuth-based compounds for use in single-junction solar cells is the wide bandgap exhibited by most materials (Table I). This could be addressed by doping or alloying to tune the band positions through changes in the composition of the density of states at the band edges. For example, it has recently been found that alloying $(CH_3NH_3)_3Bi_2I_9$ with sulfur can reduce the bandgap.[105] However, it should be noted that the bandgaps of many un-doped bismuth-based absorbers are close to the optimum for top-cells in tandems with silicon (1.7 eV for two-terminal tandems; 1.9 eV for four-terminal tandems).[4,82,110] For these applications, bismuth-based absorbers may be advantageous over lead-halide perovskites which are not photostable for bandgaps above 1.65 eV.[106]

A significant amount of effort has been invested in optimizing the morphology of bismuth-based thin films, but this has only partly addressed low device efficiencies. The intrinsic limitations in mobility and defect-tolerance of some bismuth-based absorbers (discussed in Sec. II) should be considered. Further investigation into alternative charge transport layers with improved alignment with the deep valence band maximum of bismuth-based compounds is also needed. Another important consideration is that careful selection of the contact layers is needed to achieve air-stable devices. For example, 1000 h device stability with lead-halide perovskites has been achieved under constant 1-sun illumination by using indium-tin-oxide and atomic-layer-deposited SnO_2/zinc tin oxide as the top electrode.[4] Although it has been shown that many bismuth-based absorbers are more air-stable than $CH_3NH_3PbI_3$,[3,13,39] there are no reports of 1000 h device stability. There is also no standard approach for testing and reporting the stability of bismuth-based materials or devices. For example, different storage gases (nitrogen or air), relative humidity levels, and illumination levels are used. There is also no standard test duration, which makes a comparison of the stability of materials or devices grown and tested by different research groups difficult. It is therefore important to follow protocols in stability testing. The International Summit on Organic Photovoltaics Stability (ISOS) has established protocols for the purpose of enabling accurate comparisons of reported stability and lifetime data for organic solar cells.[107] These protocols have been adopted by some groups working on lead-halide perovskites[108,109] and can be extended to bismuth-based absorbers. Research groups can utilize one of the 5 different test types prescribed in the standards (dark, outdoor, laboratory weathering testing, thermal cycling, and solar-thermal-humidity cycling) independently or in conjunction with each other for a comprehensive set of stability data. Each of the test types can be performed at three different test levels, from *basic* to *advanced* with increased levels of stringency. For example, a research group might employ the laboratory weathering protocols at the *basic level*, ISOS-L-1 whilst another group might use the same protocol but at an *advanced level*, ISOS-L-3. This allows for research groups with varying access to equipment to still report standardized measurements. For commercialization, cells will need to pass accelerated device stability tests outlined by the International Electrotechnical Committee (IEC) for terrestrial photovoltaic modules (IEC 61215-1-3:2016,

Ed. 1, 2016). These include 1000 h testing at 85 °C and 85% relative humidity under constant 1-sun illumination.

VI. CONCLUSION

Compounds containing Bi^{3+} have been proposed as having the potential to mimic the defect-tolerance of lead-halide perovskites. Detailed calculations have confirmed the predictions of high dielectric constants for many Bi-based materials, although calculations also suggest that not all compounds are defect tolerant. The recent work has shown the importance of considering electronic dimensionality, which describes the overlap between orbitals in real space and influences the effective mass and bandgap. The number of Bi-based compounds being grown as thin films is increasing, but there is still wide scope for improvements in their processing to achieve improved morphology, longer carrier lifetimes, and higher device performance. Despite this, the photoluminescence lifetimes of most of the materials have been reported to be <10 ns. There is also much scope for engineering the acceptor levels of charge transport layers to improve charge extraction. This particularly applies to hole transport layers, which need to match the deep valence band maximum positions of bismuth-based compounds.

ACKNOWLEDGMENTS

The authors would like thank Robert A. Jagt for useful discussions. L.C.L. would like to acknowledge funding from the EPSRC Centre for Doctoral Training in New and Sustainable Photovoltaics. T.N.H. acknowledges funding from the EPSRC Centre for Doctoral Training in Graphene Technology (No. EP/L016087/1). R.L.Z.H. acknowledges support from Magdalene College, Cambridge. All authors acknowledge support from the Winton Programme for the Physics of Sustainability.

[1] A. Kojima, K. Teshima, Y. Shirai, and T. Miyasaka, J. Am. Chem. Soc. **131**, 6050 (2009).
[2] See https://www.nrel.gov/pv/assets/images/efficiency-chart for National Renewable Energy Laboratory Research Cell Efficiency Records (2018).
[3] R. L. Z. Hoye, R. E. Brandt, A. Osherov, V. Stevanovic, S. D. Stranks, M. W. B. Wilson, H. Kim, A. J. Akey, J. D. Perkins, R. C. Kurchin, J. R. Poindexter, E. N. Wang, M. G. Bawendi, V. Bulovic, and T. Buonassisi, Chem. - Eur. J. **22**, 2605 (2016).
[4] K. A. Bush, A. F. Palmstrom, Z. J. Yu, M. Boccard, R. Cheacharoen, J. P. Mailoa, D. P. McMeekin, R. L. Z. Hoye, C. D. Bailie, T. Leijtens, I. M. Peters, M. C. Minichetti, N. Rolston, R. Prasanna, S. Sofia, D. Harwood, W. Ma, F. Moghadam, H. J. Snaith, T. Buonassisi, Z. C. Holman, S. F. Bent, and M. D. McGehee, Nat. Energy **2**, 17009 (2017).
[5] G. Grancini, C. Roldán-Carmona, I. Zimmermann, E. Mosconi, X. Lee, D. Martineau, S. Narbey, F. Oswald, F. De Angelis, M. Graetzel, and M. K. Nazeeruddin, Nat. Commun. **8**, 15684 (2017).
[6] A. Babayigit, A. Ethirajan, M. Muller, and B. Conings, Nat. Mater. **15**, 247 (2016).
[7] R. L. Z. Hoye, P. Schulz, L. T. Schelhas, A. M. Holder, K. H. Stone, J. D. Perkins, D. Vigil-Fowler, S. Siol, D. O. Scanlon, A. Zakutayev, A. Walsh, I. C. Smith, B. C. Melot, R. C. Kurchin, Y. Wang, J. Shi, F. C. Marques, J. J. Berry, W. Tumas, S. Lany, V. Stevanović, M. F. Toney, and T. Buonassisi, Chem. Mater. **29**, 1964 (2017).
[8] A. M. Ganose, C. N. Savory, and D. O. Scanlon, Chem. Commun. **53**, 20 (2017).
[9] Z. Xiao and Y. Yan, Adv. Energy Mater. **7**, 1701136 (2017).
[10] S. F. Hoefler, G. Trimmel, and T. Rath, Monatsh. Chem. Chem. Mon. **148**, 795 (2017).
[11] Z. Shi, J. Guo, Y. Chen, Q. Li, Y. Pan, H. Zhang, Y. Xia, and W. Huang, Adv. Mater. **29**, 1605005 (2017).
[12] C. N. Savory, A. Walsh, and D. O. Scanlon, ACS Energy Lett. **1**, 949 (2016).
[13] A. H. Slavney, T. Hu, A. M. Lindenberg, and H. I. Karunadasa, J. Am. Chem. Soc. **138**, 2138 (2016).
[14] F. Wei, Z. Deng, S. Sun, F. Zhang, D. M. Evans, G. Kieslich, S. Tominaka, M. A. Carpenter, J. Zhang, P. D. Bristowe, and A. K. Cheetham, Chem. Mater. **29**, 1089 (2017).
[15] W.-J. Yin, T. Shi, and Y. Yan, Appl. Phys. Lett. **104**, 63903 (2014).
[16] R. E. Brandt, J. R. Poindexter, P. Gorai, R. C. Kurchin, R. L. Z. Hoye, L. Nienhaus, M. W. B. Wilson, J. A. Polizzotti, R. Sereika, R. Žaltauskas, L. C. Lee, J. L. Macmanus-Driscoll, M. Bawendi, V. Stevanović, and T. Buonassisi, Chem. Mater. **29**, 4667 (2017).
[17] A. Zakutayev, C. M. Caskey, A. N. Fioretti, D. S. Ginley, J. Vidal, V. Stevanovic, E. Tea, and S. Lany, J. Phys. Chem. Lett. **5**, 1117 (2014).
[18] R. E. Brandt, V. Stevanovic, D. S. Ginley, and T. Buonassisi, MRS Commun. **5**, 265 (2015).
[19] A. Walsh and A. Zunger, Nat. Mater. **16**, 964 (2017).
[20] A. Jain, K. A. Persson, and G. Ceder, APL Mater. **4**, 53102 (2016).
[21] R. Mohan, Nat. Chem. **2**, 336 (2010).
[22] A. J. Lehner, D. H. Fabini, H. A. Evans, C. A. Hébert, S. R. Smock, J. Hu, H. Wang, J. W. Zwanziger, M. L. Chabinyc, and R. Seshadri, Chem. Mater. **27**, 7137 (2015).
[23] Z. Xiao, W. Meng, J. Wang, and Y. Yan, ChemSusChem **9**, 2628 (2016).
[24] P. Umari, E. Mosconi, and F. De Angelis, Sci. Rep. **4**, 4467 (2014).

[25] G. E. Eperon, T. Leijtens, K. A. Bush, R. Prasanna, T. Green, J. T. W. Wang, D. P. McMeekin, G. Volonakis, R. L. Milot, R. May, A. Palmstrom, D. J. Slotcavage, R. A. Belisle, J. B. Patel, E. S. Parrott, R. J. Sutton, W. Ma, F. Moghadam, B. Conings, A. Babayigit, H. G. Boyen, S. Bent, F. Giustino, L. M. Herz, M. B. Johnston, M. D. McGehee, and H. J. Snaith, Science **354**, 861 (2016).
[26] S. S. Shin, E. J. Yeom, W. S. Yang, S. Hur, M. G. Kim, J. Im, J. Seo, J. H. Noh, and S. Il Seok, Science **356**, 167 (2017).
[27] K. Eckhardt, V. Bon, J. Getzschmann, J. Grothe, F. M. Wisser, and S. Kaskel, Chem. Commun. **52**, 3058 (2016).
[28] M. Lyu, J. H. Yun, M. Cai, Y. Jiao, P. V. Bernhardt, M. Zhang, Q. Wang, A. Du, H. Wang, G. Liu, and L. Wang, Nano Res. **9**, 692 (2016).
[29] Z. Xiao, W. Meng, J. Wang, D. B. Mitzi, and Y. Yan, Mater. Horiz. **4**, 206 (2017).
[30] Z. Zhang, X. Li, X. Xia, Z. Wang, Z. Huang, B. Lei, and Y. Gao, J. Phys. Chem. Lett. **8**, 4300 (2017).
[31] S. Sun, S. Tominaka, J. H. Lee, F. Xie, P. D. Bristowe, and A. K. Cheetham, APL Mater. **4**, 031101 (2016).
[32] B. W. Park, B. Philippe, X. Zhang, H. Rensmo, G. Boschloo, and E. M. J. Johansson, Adv. Mater. **27**, 6806 (2015).
[33] F. Demartin, C. M. Gramaccioli, and I. Campostrini, Mineral. Mag. **74**, 141 (2010).
[34] A. M. Ganose, K. T. Butler, A. Walsh, and D. O. Scanlon, J. Mater. Chem. A **4**, 2060 (2016).
[35] H. Kunioku, M. Higashi, and R. Abe, Sci. Rep. **6**, 32664 (2016).
[36] N. T. Hahn, A. J. E. Rettie, S. K. Beal, R. R. Fullon, and C. B. Mullins, J. Phys. Chem. C **116**, 24878 (2012).
[37] R. E. Brandt, R. C. Kurchin, R. L. Z. Hoye, J. R. Poindexter, M. W. B. Wilson, S. Sulekar, F. Lenahan, P. X. T. Yen, V. Stevanović, J. C. Nino, M. G. Bawendi, and T. Buonassisi, J. Phys. Chem. Lett. **6**, 4297 (2015).
[38] U. H. Hamdeh, R. D. Nelson, B. J. Ryan, U. Bhattacharjee, J. W. Petrich, and M. G. Panthani, Chem. Mater. **28**, 6567 (2016).
[39] R. L. Z. Hoye, L. C. Lee, R. C. Kurchin, T. N. Huq, K. H. L. Zhang, M. Sponseller, L. Nienhaus, R. E. Brandt, J. Jean, J. A. Polizzotti, A. Kursumović, M. G. Bawendi, V. Bulović, V. Stevanović, T. Buonassisi, and J. L. Macmanus-Driscoll, Adv. Mater. **29**, 1702176 (2017).
[40] A. M. Ganose, M. Cuff, K. T. Butler, A. Walsh, and D. O. Scanlon, Chem. Mater. **28**, 1980 (2016).
[41] E. T. McClure, M. R. Ball, W. Windl, and P. M. Woodward, Chem. Mater. **28**, 1348 (2016).
[42] E. Greul, M. L. Petrus, A. Binek, P. Docampo, and T. Bein, J. Mater. Chem. A **5**, 19972 (2017).
[43] F. Wei, Z. Deng, S. Sun, F. Xie, G. Kieslich, D. M. Evans, M. A. Carpenter, P. D. Bristowe, and A. K. Cheetham, Mater. Horiz. **3**, 328 (2016).
[44] F. Viñes, M. Bernechea, G. Konstantatos, and F. Illas, Phys. Rev. B **94**, 235203 (2016).
[45] M. Bernechea, N. C. Miller, G. Xercavins, D. So, A. Stavrinadis, and G. Konstantatos, Nat. Photonics **10**, 521 (2016).
[46] D. Nason and L. Keller, J. Cryst. Growth **156**, 221 (1995).
[47] A. T. Lintereur, W. Qiu, J. C. Nino, and J. Baciak, Nucl. Instrum. Methods Phys. Res., Sect. A **652**, 166 (2011).
[48] I. P. Aleksandrov, A. F. Bovina, O. A. Ageev, and A. A. Sukhovskii, Phys. Solid State **39**, 991 (1997).
[49] S. V. Mel'nikova and A. I. Zaitsev, Phys. Solid State **39**, 1652 (1997).
[50] F. Pelle, B. Blanzat, and B. Chevalier, Solid State Commun. **49**, 1089 (1984).
[51] D. Arivuoli, F. D. Gnanam, and P. Ramasamy, J. Mater. Sci. **21**, 2835 (1986).
[52] R. Jakubas, J. Zaleski, and L. Sobczyk, Ferroelectrics **108**, 109 (1990).
[53] T. Kawai, A. Ishii, T. Kitamura, and S. Shimanuki, J. Phys. Soc. Jpn. **65**, 1464 (1996).
[54] A. Miyata, A. Mitioglu, P. Plochocka, O. Portugall, J. T.-W. Wang, S. D. Stranks, H. J. Snaith, and R. J. Nicholas, Nat. Phys. **11**, 582 (2015).
[55] M. Abulikemu, S. Ould-Chikh, X. Miao, E. Alarousu, B. Murali, G. Olivier, N. Ndjawa, E. Emy Bar, A. El Labban, A. Amassian, and S. Del Gobbo, J. Mater. Chem. A **4**, 12504 (2016).
[56] D. Shi, V. Adinolfi, R. Comin, M. Yuan, E. Alarousu, A. Buin, Y. Chen, S. Hoogland, A. Rothenberger, K. Katsiev, Y. Losovyj, X. Zhang, P. A. Dowben, O. F. Mohammed, E. H. Sargent, and O. M. Bakr, Science **347**, 519 (2015).
[57] J. Lee, B.-K. Min, I. Cho, and Y. Sohn, Bull. Korean Chem. Soc. **34**, 773 (2013).
[58] X. Su, G. Zhang, T. Liu, Y. Liu, J. Qin, and C. Chen, Russ. J. Inorg. Chem. **51**, 1864 (2006).
[59] J. Horák and K. Čermák, Czech. J. Phys. **15**, 536 (1965).
[60] L. Zhu, Y. Xie, X. Zheng, X. Yin, and X. Tian, Inorg. Chem. **41**, 4560 (2002).
[61] N. J. Podraza, W. Qiu, B. B. Hinojosa, H. Xu, M. A. Motyka, S. R. Phillpot, J. E. Baciak, S. Trolier-Mckinstry, and J. C. Nino, J. Appl. Phys. **114**, 033110 (2013).
[62] T. Saito, T. Iwasaki, S. Kurosawa, A. Yoshikawa, and T. Den, Nucl. Instrum. Methods Phys. Res., Sect. A **806**, 395 (2016).
[63] R. Jaramillo, M. J. Sher, B. K. Ofori-Okai, V. Steinmann, C. Yang, K. Hartman, K. A. Nelson, A. M. Lindenberg, R. G. Gordon, and T. Buonassisi, J. Appl. Phys. **119**, 35101 (2016).
[64] Y. N. Dmitriyev, P. R. Bennett, L. J. Cirignano, M. B. Klugerman, and K. S. Shah, Proc. SPIE **3768**, 521 (1999).
[65] H. Han, M. Hong, S. S. Gokhale, S. B. Sinnott, K. Jordan, J. E. Baciak, and J. C. Nino, J. Phys. Chem. C **118**, 3244 (2014).
[66] H. An, Y. Du, T. Wang, C. Wang, W. Hao, and J. Zhang, Rare Met. **27**, 243 (2008).
[67] V. V. Bunda and S. O. Bunda, *Superconductors—Properties, Technology, and Applications* (InTech, 2012).
[68] D. Lotnyk, V. Komanicky, V. Bunda, and A. Feher, in *18th Conference of Czech and Slovak Physicists* (2014), pp. 67–68.
[69] G. Volonakis, M. R. Filip, A. A. Haghighirad, N. Sakai, B. Wenger, H. J. Snaith, and F. Giustino, J. Phys. Chem. Lett. **7**, 1254 (2016).
[70] K. Z. Du, W. Meng, X. Wang, Y. Yan, and D. B. Mitzi, Angew. Chem., Int. Ed. **56**, 8158 (2017).
[71] J. Yang, P. Zhang, and S.-H. Wei, J. Phys. Chem. Lett. **9**, 31 (2018).
[72] C. V. Thompson, Annu. Rev. Mater. Sci. **30**, 159 (2000).
[73] R. Messier, A. P. Giri, and R. A. Roy, J. Vac. Sci. Technol., A **2**, 500 (1984).
[74] P. Barna and M. Adamik, Thin Solid Films **317**, 27 (1998).
[75] J. A. Thornton, Proc. SPIE **0821**, 95 (1988).
[76] S. Öz, J.-C. Hebig, E. Jung, T. Singh, A. Lepcha, S. Olthof, F. Jan, Y. Gao, R. German, P. H. M. van Loosdrecht, K. Meerholz, T. Kirchartz, and S. Mathur, Sol. Energy Mater. Sol. Cells **158**, 195 (2016).

[77] S. S. Shin, J.-P. Correa-Baena, R. C. Kurchin, A. Polizzotti, J. J. Yoo, S. Wieghold, M. G. Bawendi, and T. Buonassisi, Chem. Mater. **30**, 336 (2018).
[78] C. Ran, Z. Wu, J. Xi, F. Yuan, H. Dong, T. Lei, X. He, and X. Hou, J. Phys. Chem. Lett. **8**, 394 (2017).
[79] A. J. Lehner, H. Wang, D. H. Fabini, C. D. Liman, C.-A. Hébert, E. E. Perry, M. Wang, G. C. Bazan, M. L. Chabinyc, and R. Seshadri, Appl. Phys. Lett. **107**, 131109 (2015).
[80] K. Wang, F. Jia, Z. Zheng, and L. Zhang, Electrochem. Commun. **12**, 1764 (2010).
[81] K. Zhao, X. Zhang, and L. Zhang, Electrochem. Commun. **11**, 612 (2009).
[82] T. Todorov, O. Gunawan, and S. Guha, Mol. Syst. Des. Eng. **1**, 370 (2016).
[83] P.-C. Huang, W.-C. Yang, and M.-W. Lee, J. Phys. Chem. C **117**, 18308 (2013).
[84] S. Zhou, J. Yang, W. Li, Q. Jiang, Y. Luo, D. Zhang, Z. Zhou, and X. Li, J. Electrochem. Soc. **163**, D63 (2016).
[85] N. Liang, W. Chen, F. Dai, X. Wu, W. Zhang, Z. Li, J. Shen, S. Huang, Q. He, J. Zai, N. Fang, and X. Qian, CrystEngComm **17**, 1902 (2015).
[86] C. Zuo, H. J. Bolink, H. Han, J. Huang, D. Cahen, and L. Ding, Adv. Sci. **3**, 1500324 (2016).
[87] N. Elumalai, M. Mahmud, D. Wang, and A. Uddin, Energies **9**, 861 (2016).
[88] Z. Fan, K. Sun, and J. Wang, J. Mater. Chem. A **3**, 18809 (2015).
[89] M. B. Johansson, H. Zhu, and E. M. J. Johansson, J. Phys. Chem. Lett. **7**, 3467 (2016).
[90] M. Cai, Y. Wu, H. Chen, X. Yang, Y. Qiang, and L. Han, Adv. Sci. **4**, 1600269 (2017).
[91] P. Vivo, J. K. Salunke, and A. Priimagi, Materials **10**, 1087 (2017).
[92] J.-H. Kim, I. Lee, T.-S. Kim, N. Rolston, B. L. Watson, and R. H. Dauskardt, MRS Bull. **42**, 115 (2017).
[93] M. Yang, Z. Shi, J. Feng, H. Pu, G. Li, J. Zhou, and Q. Zhang, Thin Solid Films **519**, 3021 (2011).
[94] G. Li, Y. Jiang, S. Deng, A. Tam, P. Xu, M. Wong, and H. S. Kwok, Adv. Sci. **4**, 1700463 (2017).
[95] S. Chen, J. R. Manders, S.-W. Tsang, and F. So, J. Mater. Chem. **22**, 24202 (2012).
[96] P. Schulz, J. O. Tiepelt, J. A. Christians, I. Levine, E. Edri, E. M. Sanehira, G. Hodes, D. Cahen, and A. Kahn, ACS Appl. Mater. Interfaces **8**, 31491 (2016).
[97] X. Gu, W. Cui, H. Li, Z. Wu, Z. Zeng, S.-T. Lee, H. Zhang, B. Sun, X. Gu, W. Cui, Z. W. Wu, S. Lee, B. Q. Sun, H. Li, Z. Y. Zeng, and H. Zhang, Adv. Energy Mater. **3**, 1262 (2013).
[98] D. Ovchinnikov, A. Allain, Y.-S. Huang, D. Dumcenco, and A. Kis, ACS Nano **8**, 8174 (2014).
[99] A. Capasso, F. Matteocci, L. Najafi, M. Prato, J. Buha, L. Cin, V. Pellegrini, A. Di Carlo, and F. Bonaccorso, Adv. Energy Mater. **6**, 1600920 (2016).
[100] P. Huang, Z. Wang, Y. Liu, K. Zhang, L. Yuan, Y. Zhou, B. Song, and Y. Li, ACS Appl. Mater. Interfaces **9**, 25323 (2017).
[101] Y. G. Kim, K. C. Kwon, Q. Van Le, K. Hong, H. W. Jang, and S. Y. Kim, J. Power Sources **319**, 1 (2016).
[102] K. Mahmood, S. Sarwar, and M. T. Mehran, RSC Adv. **7**, 17044 (2017).
[103] W. S. Yang, B.-W. Park, E. H. Jung, and N. J. Jeon, Science **356**, 1376 (2017).
[104] X. Zhang, G. Wu, Z. Gu, B. Guo, W. Liu, S. Yang, T. Ye, C. Chen, W. Tu, and H. Chen, Nano Res. **9**, 2921 (2016).
[105] M. Vigneshwaran, T. Ohta, S. Iikubo, G. Kapil, T. S. Ripolles, Y. Ogomi, T. Ma, S. S. Pandey, Q. Shen, T. Toyoda, K. Yoshino, T. Minemoto, and S. Hayase, Chem. Mater. **28**, 6436 (2016).
[106] E. T. Hoke, D. J. Slotcavage, E. R. Dohner, A. R. Bowring, H. I. Karunadasa, and M. D. McGehee, Chem. Sci. **6**, 613 (2015).
[107] M. O. Reese, S. A. Gevorgyan, M. Jørgensen, E. Bundgaard, S. R. Kurtz, D. S. Ginley, D. C. Olson, M. T. Lloyd, P. Morvillo, E. A. Katz, A. Elschner, O. Haillant, T. R. Currier, V. Shrotriya, M. Hermenau, M. Riede, K. R. Kirov, G. Trimmel, T. Rath, O. Inganäs, F. Zhang, M. Andersson, K. Tvingstedt, M. Lira-Cantu, D. Laird, C. McGuiness, S. Gowrisanker, M. Pannone, M. Xiao, J. Hauch, R. Steim, D. M. Delongchamp, R. Rösch, H. Hoppe, N. Espinosa, A. Urbina, G. Yaman-Uzunoglu, J. B. Bonekamp, A. J. J. M. Van Breemen, C. Girotto, E. Voroshazi, and F. C. Krebs, Sol. Energy Mater. Sol. Cells **95**, 1253 (2011).
[108] E. M. Sanehira, B. J. Tremolet De Villers, P. Schulz, M. O. Reese, S. Ferrere, K. Zhu, L. Y. Lin, J. J. Berry, and J. M. Luther, ACS Energy Lett. **1**, 38 (2016).
[109] E. Zimmermann, K. K. Wong, M. Müller, H. Hu, P. Ehrenreich, M. Kohlstädt, S. Mastroianni, G. Mathiazhagan, A. Hinsch, T. P. Gujar, M. Thelakkat, T. Pfadler, and L. Schmidt-Mende, APL Mater. **4**, 91901 (2016).
[110] R. L. Z. Hoye, K. A. Bush, F. Oviedo, S. E. Sofia, M. Thway, X. Li, Z. Liu, J. Jean, J. P. Mailoa, A. Osherov, F. Lin, A. F. Palmstrom, V. Bulović, M. D. McGehee, I. M. Peters, and T. Buonassisi, IEEE J. Photovolt. (published online).
[111] R. L. Z. Hoye, L. Eyre, F. Wei, F. Brivio, A. Sadhanala, S. Sun, W. Li, K. H. L. Zhang, J. L. MacManus-Driscoll, P. D. Bristowe, R. H. Friend, A. K. Cheetham, and F. Deschler, Adv. Mater. Interfaces (in press).